IOSR Journal Of Pharmacy And Biological Sciences (IOSR-JPBS)
e-ISSN:2278-3008, p-ISSN:2319-7676. Volume 14, Issue 1 Ser. IV (Jan – Feb 2019), PP 08-20
www.Iosrjournals.Org

In-Silico Analysis, Catalytic Site and Substrate Specificity Prediction of Two Phylogenetically Distinct Zea mays Allene Oxide Synthases

Eman Wahba Elgammal [1], Heba Shawky [2 *], Michael V. Kolomiets [3]
[1]*Department of Chemistry of Natural and Microbial Products, Division of Pharmaceutical Industries and Drug, National Research Centre, Dokki, Giza 12622, Egypt*
[2]*Department of Therapeutic Chemistry, Division of Pharmaceutical Industries and Drug, National Research Centre, Dokki, Giza 12622, Egypt*
[3]*Department of Plant Pathology and Microbiology, Texas A&M University, College Station, TX, USA*
**Corresponding author: Eman Wahba Elgammal*

Abstract: *Allene oxide synthase (AOS) is a member of CYP74A subfamily of the P450 enzyme superfamily that plays an important role in biosynthesis of oxylipins, which exhibit signaling and defense functions in mammals, plant, algae and fungi. The main objective of this report is to characterize the structural features of two Zea mays AOS genes (AOS_2b and 1c) that phylogenetically belong to separate clades of the same subfamily through computational methods. Tertiary models of both proteins were generated and evaluated, and both showed good quality in different energy and conformation assessments. The modeled enzymes showed all unique characteristics of other P450 proteins members – AOSs in particular – including the P450 functional heme-domain and the highly conserved heme-iron ligand Cysteine residues. Through molecular docking simulation, the modeled proteins exhibited preferential affinities toward different substrates, with AOS-1c model being more interactive with the screened substrates than AOS-2b model. Both enzymes surpassed the reference models and formed stronger interactions and more stable complexes in terms of full fitness and binding energy. The catalytic residues involved in the complex formation were also predicted. In conclusion, the present study represents the first report on systematic characterization of Zea mays AOS enzymes structural features given that the majority of well refined models of such enzyme belong to other plant species.*

Keywords: *Zea Mays, Allene Oxide Synthase (AOS), In-Silico Analysis, Molecular Docking, Substrate Specificity, Catalytic Residues.*

Date of Submission: 30-01-2019 Date of acceptance:16-02-2019

I. Introduction

Cytochrome P450 (CYP) enzymes are heme-containing monooxygenase superfamily that is found in all kingdoms of life, catalyzing a wide range of chemical reactions. They play important roles in detoxification processes, drug metabolism, cholesterol synthesis, controlling hormone level, and also involved in vascular auto-regulation especially in the brains of mammals. In addition, they are involved in the biosynthesis of hormones, defense-related compounds in plants, and synthesis of antibiotics in bacteria **[1].** The CYP74 family enzymes are non-classical enzymes because they do require neither oxygen nor NADPH-reductase in their reactions. Consequently, they have extraordinarily high catalytic centre activities [**2].** Allene oxide synthase (AOS) is a member of CYP74A subfamily that plays an important role in the biosynthesis of oxidized fatty acids (oxylipins), a group of biologically active molecules that are implicated in having signaling and antimicrobial activities in mammals, plants, algae and fungi **[3, 4]**. Regarding substrate preference, the majority of CYP74A subfamily enzymes utilize 13(*S*)-hydroperoxides as substrates by catalyzing a dehydration reaction to convert 13(*S*)-hydroperoxides, derived from linolenic acid by lipoxygenase to allene oxide, which is further cyclized by allene oxide cyclase. The AOS branch of the LOX pathway eventually leads to the formation of jasmonic acid (JA), a major plant defense hormone **[5]**. The AOS isozymes involved in JA biosynthesis are designated as "13-AOSs" **[6]**, whereas 9/13- and 9-AOSs are grouped in the CYP74C subfamily **[7]**.

Structural studies of P450s provide an essential basis for understanding their complex catalytic reactions. To date, many structures have been reported for bacteria **[8],** eukaryotes, several mammalian microsomal P450 structures. However, only few plants' P450 or AOS structures have been characterized **[9].** Homology modeling of AOSs is reportedly problematic because of the poor sequence identity with any other P450 enzymes. Detailed structural information is therefore essential to understand the catalytic mechanisms of AOS. In light of the scarcity of literature that tackles the structural properties and catalytic mechanisms of *Zea*

mays AOSs, this report aimed at systematic characterization of two phylogenetically distinct AOS genes cloned from *Zea mays*. Multiple computational methods were used to predict the structural features, substrate specificity and identify the catalytic residues involved in complex formation with different substrates.

II. Computational Methods

Sequence Alignment Comparison and Analysis

Two fragments encoding *Zea mays* allene oxide synthase active enzyme were successfully amplified, cloned in pSC-A PCR cloning vector **(Stratagen, US)** and subjected to automated DNA sequence analysis in **Geospiza, Germany.** The cloned amplicons full length sequence was analyzed using BLAST algorithm available at http://www.ncbi.nlm.nih.gov. Nucleotide sequences were aligned against NCBI DataBase using megablast analysis optimized for highly similar sequences, while translated nucleotide sequences were aligned against both non-redundant data bases (nrdb) and Protein Data Bank using PSI-BLAST **[10].** Construction of a neighbor-joining phylogenetic tree was carried out using the Bioedit software (http://www.mbio.ncsu.edu/BioEdit/). Different parameters of primary structure analysis were computed using ProtParam online tool **[11].** Sequence-based secondary structure predictions were carried out using PREDICT-PROTEIN **[12]** and PDBsum online server that performs a sequence-based search of a given protein sequence against all sequences in PDB protein structure database **[13].** The predicted secondary structures were further analyzed for folding homology using Phyre2 protein homology/analogy recognition engine **[14].**

Tertiary Structure Model Building, Refinement and Validation

The resulting consensus secondary structure prediction was used as a template for the homology-modeling SWISS-MODEL server **[15]** to generate the threading alignment according to protein structures in PDB database having the same folding of the target protein. The model with the best global model quality estimation (GMQE) and QMEAN (degree of nativeness) scores were selected for refinement and validation. GMQE-score that lies between 0-1 and QMEAN Z-score that lies within range of -4 and 4 signifies a model with a good quality. The generated model was then submitted to the protein structure refinement server $3D^{refine}$ (http://sysbio.rnet.missouri.edu/$3D^{refine}$) for energy minimization and hydrogen bonding network optimization. Refined models were then subjected to structural and stereo-chemical assessment using a suite of predictors including PROCHECK **[16],** WHAT_CHECK **[17],** ERRAT **[18]**, VERIFY_3D **[19]**, PROVE **[20]**, CRYST1 record matches and Psi/Phi Ramachandran plot that evaluates backbone conformation and assess the model quality in terms of Z-scores indicative of overall model quality and to assure that the predicted structure is within the range of score as found in native proteins; all integrated in the Structure Analysis and Verification Server (http://services.mbi.ucla.edu/SAVES/).

Functional Annotation and Binding Site Prediction

The functional assessment of the predicted models was carried out by searching against Pfam database. Active site residues and ligand binding site of the modeled structures was determined by RaptorX (http://raptorx.uchicago.edu/) and CASTp **[21]** servers respectively.

Molecular Docking

Modeled AOSs were analyzed for molecular docking with three specific substrates, namely, 13S-hydroperoxy-9Z,11E-octadecadienoic acid (13(S)-HPODE); 9-hydroperoxy-11,12-octadecadienoic acid (9(S)-HPODE) and 13-hydroperoxy-9,11,15-octadecatrienoic acid (13(S)-HpOTrE) in Swiss-Dock energy scoring web server **[22].** The docking process from Swiss-Dock was set to the accurate type and since the docking was flexible Definition of the region of interest was set as default. The allowance for the flexibility for side chains was set to within 0 Å of any atom of the ligand in its reference binding mode. To recognize binding residues involved in interacting with each substrate, GALAXY 7TM web server **[23]** was employed. To generate and select the models, refinement energy and docking energy were used and top10 conformations were selected by the sum of rank in refinement energy and half of the rank in docking energy. This score was trained to predict the docking accuracy, and the models were ordered by this score with ligand RMSD value provided.

III. Results

Sequence and Phylogenic Analysis of Amplified AOS Fragments

Because of the recently proposed nomenclature of maize jasmonic acid biosynthesis enzymes **[24]**, the sequences cloned in this study were designated as AOS1c and AOS2b. Blast analysis of the amplified AOS-2b sequences revealed partial homology with previously published sequences of AOS in different plant species , including *Sorghum bicolor* (XM_002468192), *Setaria italica* (XM_004985083), *Triticum aestivum* (KF039886), *Aegilops tauschii* (XM_020292469), *Brachypodium distachyon* (XM_003558398), *Hordeum vulgare* (AJ250864), *Aegilops tauschii* (XM_020292468), and *Oryza sativa Japonica* (XM_015773277). The

highest homology was annotated with the sequence from *Zea mays* AOS1 (aos1) mRNA (NM_001111774.2) with 96% sequence identity covering 99% of the query sequence. In contrast, AOS1c fragment sequence revealed partial homology with mostly "predicted" sequences rather than "amplified". The highest homology was annotated with [Predicted] sequence of *Zea mays* AOS1, chloroplastic (LOC103625850), mRNA (XM_008646248), with 91% sequence identity covering 98% of the query sequence. This allowed us to conclude that the cloned AOS1c encoding sequence is a novel one. Interestingly, when our AOS1c and AOS2b sequences were aligned against each other the blast showed only 70% and 47% nucleotide and amino acid identity, respectively, thus confirming that these two enzymes belong to two separate clades. Neighbor-joining phylogenetic tree of both sequences is demonstrated in **Fig**. **(1)**.

Sequence-Based Features Of AOS Proteins

Predicted physiochemical parameters of AOS proteins primary structures showed that they are composed of 387 and 493 amino acids corresponding to molecular weights of 42.7 and 55.2kDa for AOS2b and AOS1c, respectively. The calculated isoelectric point (pI) of AOS2b was 7.68, with 44 negatively charged residues and 45 positively charged residues, indicating that it tends to have a neutral charge. AOS1c has a pI value of 9.84 with 52 negatively charged residues and 70 positively charged residues, reflecting the alkaline property of the protein. The computed instability index (II) for AOS2b was 26.19, which reflects the stability of the protein with a calculated half-lifetime of more than 10 hours in prokaryotes and 30 hours in eukaryotic cells (*in vitro*), while AOS1c was classified as unstable with an instability index value of 47.19 and a similar half-lifetime in prokaryotes but only 4.4 hours in eukaryotic cells. AOS2b protein has an N-terminus M (Met) residues, while AOS1c has A (Ala) N-terminus, and both have a negative grand average of hydropathicity (GRAVY) values as -0.080 and -0.312 for 2b and 1c, respectively, indicating that they both are hydrophilic.

Secondary structure analysis showed that both proteins are largely comprised of ά-helix and loops with traces of ß-turns and strands, where AOS2b consists of 47.03% helix, 48.06% loops, and 4.91% strands, while AOS1c comprises of 40.97% helix, 53.96% loops, and 5.07% strands. Both proteins also incorporate 3 transmembrane helices (13.9%) necessary for membrane localization and sub-cellular targeting. As for protein accessibility, 36.43% of AOS2b structure is exposed, 52.2% buried and 11.37% intermediate, whereas 38.54% of AOS1c is exposed, 52.74% buried and 8.72% intermediate. As evident from the predicted secondary structures, the two AOSs share similar features with slight difference that lies in the number of residues interacting with N-octane ligand (OCT). In AOS2b, the OCT ligand interacts with three residues, namely Trp124, Leu142 and Leu143 with 7 non-bonded contacts, while in AOS1c. This ligand interacts with four residues, Thr226, Pro235, Leu237, Leu488 with 11 non-bonded contacts. Interestingly, multiple-sequence alignments of the two proteins against the NCBI Conserved Protein Domain Family database **(Fig. 2)** reveled that they share some structural features with other P450 superfamily members other than AOSs, including crystal structure of human cyp11a1 in complex with cholesterol (PDB: 3N9Y.A), mitochondrial cholesterol side-chain cleavage enzyme (UniProtKB/Swiss-Prot: Q07217.1) among others; and despite the high level of primary sequence heterogeneity, the highly conserved heme-binding loop (residues 217-352 in AOS2b with E-value: 2.32e-08; residues 331-477 in AOS1c with 3.15e-11) was well conserved in our protein structures **Fig (5.B, D)**. Subcellular localization was also predicted by PREDICT-PROTEIN online server, revealing that both proteins are localized in chloroplast of *Arabidopsis thaliana* and *Zea mays* among other plants; with prediction confidence score 42 and 46 for AOS2b and 1c respectively, where confidence score ranges from 0=unreliable to 100=reliable. However, Target P prediction software did not support chloroplast localization of AOS2b; while clearly indicate plastid localization of AOS1c.

Tertiary Structure Building, Validation and Quality Assessment

Based on model-template alignment against the SWISS-MODEL template library, consensus secondary structures of AOS2b and 1c were used as templates to generate the threading alignment and build the tertiary structures of two proteins. The generated models showed good quality in terms of GMQE and QMEAN Z-scores, as AOS2b model scored 0.78 and -1.79 respectively, whereas the 1c model had 0.72 and -1.98 scores. In general, both proteins were found structurally similar to other P450 AOSs, with the highest similarity annotated to the crystal structure of *Arabidopsis thaliana* AOS belonging to the CYP74A complexed with 13(S)-HOT at 1.60 Å resolution (PDB: 3dsi.A). Superimposing our AOS models with the 3dsi.A template **(Fig. 3.A, B)** gave a RMSD value of 0.30, 0.54Å with 381 (2b), 454 residues (1c) aligned. Both models were then subjected to refinement and validation, and the refined models showed an overall high quality in ERRAT and PROVE evaluations **(Table 1).** Both models similarly passed the VERIFY3D evaluation with 87.50% (2b) and 97.38% (1c) of the residues having an averaged 3D-1D score $\geq$ 0.2, suggesting that the predicted tertiary structures are of good quality. Moreover, Z-score **(Fig. 4.A, B)** calculated by ProSA-web server indicated that the predicted models overall quality lies within the score range of experimentally determined protein tertiary structures by X-ray and NMR crystallography. Ramachandran Plot results also confirmed the quality of the

generated structures, where it revealed that the residues in AOS_2b and 1c models are in the most favored region **(Fig. 4.C and D)**.

Functional Annotation, Domain Conservation and Binding Site Prediction

For functional annotation, the generated models were submitted in ProFunc web server, and both proteins were characterized as "Cytochrome P450" with P450 motif PF00067 determined within residues 185-379 of AOS2b model (E-value 1e-104), and within AOS1c residues 327-482 (E-value 5e-84). For visualization, the two models were searched in the Pfam conserved domains database through POLYVIEW-3D interface **(Fig. 5.A, C).** Heme domain was also determined in the modeled structures, matching the atomic structure of the heme domain of flavocytochrome p450- bm3 (PDB: 2ij2) in the AOS2b model with E-value 1.237 and the crystal structure analysis of a 6-coordinated cytochrome p450 from *Thermus thermophilus* hb8 (PDB: 1wiy) in AOS1c model with E-value 0.123. Notably, the generated models were submitted in ProFunc web server, and both proteins were characterized as "Cytochrome P450" with P450 motif PF00067 determined within residues 185-379 of AOS2b model (E-value 1e-104), and within AOS1c residues 327-482 (E-value 5e-84). For visualization, the two models were searched in the Pfam conserved domains database through POLYVIEW-3D interface **(Fig. 5.A, C).**

Heme domain was also determined in the modeled structures, matching the atomic structure of the heme domain of flavor-cytochrome p450- bm3 (PDB: 2ij2) in the AOS2b model with E-value 1.237 and the crystal structure analysis of a 6-coordinated cytochrome p450 from *Thermus thermophilus* hb8 (PDB: 1wiy) in AOS1c model with E-value 0.123. Notably, the matched residues in our modeled structures with these templates included the highly conserved Cys residue serving as the 5th ligand of heme iron; Cys 347 and Cys 455 in 2b and 1c models respectively **Fig (5.B, D)**. Substrate binding pockets of our modeled structures were determined by CASTp server with a volume cut-off 500Å included. Modeled AOS2b was shown to incorporate three pockets; the largest is located in a cavity of 5778 Å^3 volume that lies between α1, α11 and α22 helices, and a second pocket of the same volume located in 3920 Å^3 cavity in the posterior level of first pocket within two C sheets of the 3rd strand and a smaller third pocket located in a cavity of 1617.47 Å^3 lying between α3 and α22 and overlapping with the first pocket **(Fig. 6.A)**. For AOS1c, two pockets were detected, a large pocket that lies in a cavity of 13900 Å^3 located between α6, α10 and α15 helices **(Fig. 6.B).** As expected, the interacting pocket residues in both models encompassed the hem-domain, which came in accordance with previous studies that reported the significance of hem in AOSs catalytic activity **[7].** Heme domain and substrate binding **r**esidues of both models are listed in **Table (2).**

Molecular Docking

In these simulations, we aimed to assess the binding affinity of our modeled protein to indicate the CYP74 subgroup to which they belong, and find out whether any of the screened substrates has a selective affinity to the modeled AOSs. The estimated binding energy difference between the complex and free enzyme and ligands was used to assess the strength of interaction. For quality assessment of the obtained data, a reference model (PDP: 3dan) of known binding affinity was included. This template in particular was selected for two reasons; first, it represents a well defined crystal structure of native AOS unlike most of PDB deposited AOS structures that are already complexed with a substrate. Secondly, it showed high structural similarity with our models in TM-alignment evaluation, where AOS2b scored RMSD 0.86 Å with 384 residues aligned, while the 1c model scored RMSD 0.51Å with 463 residues aligned. Using Swiss-Dock energy scoring interface, all of the screened substrates were successfully docked within the active site of the modeled AOSs in the appropriate poses with close distance of C13-hydroxyl group to heme-iron atom **(Fig.7);** showing varying binding affinities that were generally higher than those of the reference structure **(Fig. 8.A).** Binding energy data suggested that reference structure has a stronger affinity to 13(*S*)-HPODE and HpOTrE (ΔG: -8.92, -8.52 kcal/mol respectively) than to the 9(*S*)-isomer (ΔG: -7.43 kcal/mol), which agrees with being a member of CYP74 (A) – AOSs known to solely utilize the 13(S)-hydroperoxides **[6]** and further reflect the accuracy of obtained data. Compared to the reference model, the modeled AOSs have dual specificity to both 9 and 13- hydroperoxides, which imply that they belong to 9/13-CYP74 (C) AOSs; yet, AOS1c was more interactive forming more stable complexes with higher affinities. This observation was distinctive from the interactions of AOS2b where there is no significant difference in binding affinities to the screened substrates with only better fitness with 13(S)-HPODE compared to the other substrates with nearly the same binding energies. Such discrepancy of binding affinities between the two models might be attributed to the considerable variation in the primary structure composition and structural motifs of the two proteins given that they originate from two different clades. It was also observed that AOS1c docked with 9(S)-HPODE was recorded as the most favorable binding energy (ΔG: -9.09 kcal/mol) compared to AOS2b (ΔG: -8.63 kcal/mol) and reference model (ΔG: -7.43 kcal/mol), followed by 13(S) – HPODE (ΔG: -8.74 kcal/mol) **(Fig. 8.B)**.

Prediction of Catalytic Residues and Complex Interactions

Docked substrate poses were further scrutinized for their ability to reproduce similar interactions within their modeled receptors as those observed in crystal structures. The preferential affinity of modeled AOSs was elucidated in these simulations, where the relatively similar affinity of AOS2b toward the screened substrates was revealed as comparable hydrogen binding to active site residues. In descending order considering the binding energies, 13(S)-HPODE transposed in the active site forming two hydrogen bonds of the same length (3.12 Å) with the conserved Cys 347 residue and Asn 333 **(Fig. 9.A)**, while 9(S)-HPODE transposed by forming two hydrogen bonds with Lys 6 (2.79 Å) and Asn 333 (2.94 Å) **(Fig. 9.B),** and two hydrogen bonds almost of the same length (3.08 Å) connected 13(S)-HpOTrE with Lys 6 residue **(Fig. 9.C).** In AOS1c model, the highest affinity toward 9(S)-HPODE was revealed as three hydrogen bonds, one formed by the substrate with Gln 375 (3.09 Å) and two with Lys 115 (3.09, 3.35 Å) **(Fig. 9.D),** followed by 13(S)-HPODE that formed two hydrogen bonds with Gln 345 (3.23 Å) and Lys 453 (3.09 Å) **(Fig. 9.E),** while 13(S)-HpOTrE was transposed by forming two bonds with the conserved Cys 455 (3.21 Å) and Ala 456 residues **(Fig. 9.F).** As for the reference model, the results came in accord with its cognate-ligand interactions in the crystal structure, where the highest affinity was annotated to 13(S)-HPODE that transposed in the active site forming three hydrogen bonds with Asn 276 (3.15 Å), Gly 428 (2.92 Å) and the conserved Cys 426 ligand (3.04 Å) **(Fig. 9.G)** followed by 13(S)-HpOTrE that transposed in the active site forming two hydrogen bonds with Gln 347 (3.01, 3.09 Å) **(Fig. 9.H),** while the weakest interaction was shown with 9(S)-HPODE that merely transposed with hydrophobic contacts in the distal side of heme-ligand plane **(Fig. 9.I).** As evident from these results, the catalytic residues in all the screened complexes encompass the heme-ligand biding residues, particularly the conserved Cysteine heme-iron ligand. The catalytic residues involved in complex formation are listed in **Table (3).**

IV. Discussion

Most of the computational methods used for predicting protein structure rely on homology with previously characterized proteins. However, homology-based methods usually fail to discover truly novel protein structures. Considering that a limited volume of research have been carried out on structural features of *Zea mays* AOS, combined with the unavailability of high resolution structures of the *Zea mays* AOS the Protein Data Bank (PDB) (http://www.rcsb.org/pdb/home); this work represent the first inclusive systematic report that characterize the structural features of two *Zea mays* AOS domains that originate from different clades. To achieve this, two genes representing two different clades of AOS were amplified, sequenced and blasted for homology against published sequences of NCBI database. The amplified sequences showed a high similarity with AOS primary structure composition, and reasonable identity of secondary structural element, but also maintained the P450 functional domain. Tertiary structures were also generated and validated and both were within expected ranges for well-refined structures as revealed by ProsA scores corresponding to the chi-1/chi-2 angles, backbone conformation. Ramachandran plot evaluation also showed good quality models with more than 95% of residues in the most favorable region.

Although cytochrome P450s generally catalyze an enormously wide range of chemical reactions and have different enzymatic mechanisms and complex substrate specificities, AOS enzymes possess a distinctive structural feature that defines a heme-mediated substrate binding mode. In this mode, 13(*S*)-hydroperoxide substrate binds to the heme iron via the C13-oxygen atom **[7]**, and therefore, the distance between heme-iron and substrate C13/C9-oxygen is a determinant of substrate recognition and catalysis mechanisms in AOSs. In this context, three standard substrates were screened for molecular docking with the modeled structures for substrate recognition and binding affinity assessments, along with a reference model to ensure the quality of obtained results. For that, all models were first subjected to a second round of energy minimization that included fixing side chains, protonation and adding missing charges. Both models proved reactive with comparable energy profiles with the reference, only the screened substrates, particularly 9(S)-HPODE seem to interact more strongly with modeled AOS1c. Moreover, the varying affinities of our models along with the reference structure toward the screened substrates were elucidated in terms of C9/13-Oxygen distance from heme-iron atom, where the strong affinity of AOS2b to 13(S)-HPODE and AOS1c to 9(S)-analog was interpreted by the transposition modes in which substrate C13/C9-Oxygen was closest to heme-iron atom (3.954, 6.113Å respectively), and similarly with the lowest affinity of reference model to 9(S)-HPODE that transposed away of such atom (15.798 Å). Despite the structural similarity of many P450 enzymes, that would necessitate complex formation involving certain interactive residues in the binding site, it was observed that catalytic residues in the modeled AOSs are distinct from those in the reference model. Still, there were several residues that were involved in complex formation with different substrates in each model, including Asn 196, Val 263, Asn 33 in AOS2b, and Phe 119, Val 372, Asn 441, and all encompassed heme-binding residues. Notably, the conserved heme-cofactor ligand Cys residues (347 in 2b, 455 in 1c) corresponding to Cys 426 in reference models were also maintained whether through hydrogen binding or hydrophobic interactions with screened substrates. The rigid nature docking is one limitation of this study because dynamic effects of binding during complex formation are not accounted for.

Further investigations using molecular dynamics simulations are underway to dynamically test the stability and hydrogen bonding network responsible for complexes. Specifically, it will be important to understand how the flexibility and dynamic motions of both ligand and enzyme will affect the interactions using molecular dynamics simulations.

Competing Interests
The authors declare that they have no competing interests with others.

Acknowledgements

The authors acknowledge the Science & Technology Development Fund (STDF) for providing funds required to achieve this work and also the National Research Centre (NRC) of Egypt for providing all required facilities and logistics for the work.

Author Contribution
Kolomiets V.M. and Elgammal E.W. together with Shawky H. proposed and designed the study. Shawky H. performed the computational methods and wrote the manuscript along with Elgammal E.W.

Funding
This work was supported by STDF in house grants provided to Eman W. Elgammal.

References

[1]. Isin E.M., Guengerich F.P. (2007). Complex reactions catalyzed by cytochrome P450 enzymes. *Biochim Biophys Acta;* 1770:314–329.
[2]. Song W.C., Funk C.D. and Brash A.R. (1993). Molecular cloning of an allene oxide synthase: a cytochrome P450 specialized for the metabolism of fatty acid hydroperoxides. Proc. Natl. Acad. Sci. USA; 90: 8519–8523.
[3]. Pohnert G. (2005). Diatom/copepod interactions in plankton: The indirect chemical defense of unicellular algae. *Chembiochem;* 6:1–14.
[4]. Brodhun F. and Feussner I. (2011). Oxylipins in fungi. FEBS J.; 278:1047–1063.
[5]. Veldink G.A., Vliegenthart J.F.G. and Boldingh J. (1970): The enzymic conversion of linoleic acid hydroperoxide by flax-seed hydroperoxide isomerase. Biochem. J.; 120: 55–60.
[6]. Stumpe M., Feussner I. (2006). Formation of oxylipins by CYP74 enzymes. *Phytochem Rev;* 5:347–357.
[7]. Li L., Chang, Z., Pan, Z., Fu Z.Q. and Wang X. (2008). Modes of heme binding and substrate access for cytochrome P450 CYP74A revealed by crystal structures of allene oxide synthase. *Proceedings of the National Academy of Sciences*; *105*(37): 13883-13888.
[8]. Podust L.M., Poulos T.L. and Waterman M.R. (2001). Crystal structure of cytochrome P450 14alpha -sterol demethylase (CYP51) from *Mycobacterium tuberculosis* in complex with azole inhibitors. Proc. Natl. Acad. Sci. USA; 98(6):3068–3073.
[9]. Yan J.K., Hsu M.H., Griffin K.J., Stout C.D. and Johnson E.F. (2005). Structures of human microsomal cytochrome P450 2A6 complexed with coumarin and methoxsalen. *Nat Struct Mol Biol;* 12:822–823.
[10]. Altschul, S.F., Madden, T.L., Schaffer, A.A., Zhang, J., Zhang, Z., Miller, W. and Lipman, D.J. **(**1997). Gapped BLAST and PSI-BLAST: a new generation of protein database search programs. *Nucleic Acids Res*, 25: 3389-402.
[11]. Wilkins M.R., Gasteiger E., Bairoch A., Sanchez J.C., Williams K.L., Appel R.D. and Hochstrasser D.F. (1999). Protein identification and analysis tools in the ExPASy server. *Methods Mol Biol*; 112: 531–52.
[12]. Rost B. (1996). PHD: predicting one-dimensional protein structure by profile-based neural networks. Methods Enzymol; 266: 525-39.
[13]. de Beer T.A.P., Berka K., Thornton J.M. and Laskowski R.A. (2014). PDBsum additions. *Nucleic Acids Res.*; 42, D292-D296.
[14]. Kelley L.A., Mezulis S., Yates C.M., Wass M.N., Sternberg M.J. (2015). The Phyre2 web portal for protein modelling, prediction and analysis. Nature protocols; 10(6):845-858.
[15]. Guex N. and Peitsch M.C. (1997). SWISS-MODEL and the Swiss-PdbViewer: An environment for comparative protein modeling. *Electrophoresis;* 18, 2714-2723.
[16]. Laskowski R.A., MacArthur M.W., Moss D.S. and Thornton J.M. (1993). PROCHECK - a program to check the stereochemical quality of protein structures. *J App Cryst*, 26 (2):283–91.
[17]. Hooft R.W.W., Vriend G., Sander C. and Abola E.E. (1996). Errors in protein structures. Nature; 381, 272-272.
[18]. Colovos C. and Yeates T.O. (1993). Verification of protein structures: patterns of nonbonded atomic interactions. *Protein Science : A Publication of the Protein Society*; 2(9):1511-1519.
[19]. Lüthy R., Bowie J.U., Eisenberg D. (1992). Assessment of protein models with three-dimensional profiles. Nature; 356(6364):83-85.
[20]. Pontius J., Richelle J., Wodak S.J. (1996). Deviations from standard atomic volumes as a quality measure for protein crystal structures. J. Mol. Biol.; 264(1):121-136.
[21]. Dundas J., Ouyang Z., Tseng J., Binkowski A., Turpaz Y. and Liang J. (2006). CASTp: Computed Datas of Surface Topography of Proteins with Structural and Topographical Mapping of Functionally Annotated Residues, Nucleic Acids Research, 34, W116-W118.
[22]. Grosdidier A., Zoete V. and Michielin O. (2011). SwissDock, a protein-small molecule docking web service based on EADock DSS. Nucleic Acids Research; 39 (Web Server issue):W270-W277.
[23]. Lee G.R. and Seok C. (2016). Galaxy7TM**:** flexible GPCR–ligand docking by structure refinement. Nucleic Acids Research; 44 (Issue W1): W502–W506.
[24]. Borrego E.J. and Kolomiets M.V. (2016). Synthesis and Functions of Jasmonates in Maize. Wurtele E.S., ed. *Plants*, 5(4):41.

Table (1): Quality Assessment and Validation of Our Modeled AOSs

Model	Template ID	% Identity	Coverage	Superimposition TM- score (0.5 < TM-score < 1.00, in about the same fold)	PROVE Z- Score	ERRAT Score	ProsA Z-score	Ramachandran plot score (> 90% indicate good model)
AOS_2b	3dsi.A	53.28	98%	0.99047	1.547	90.489	-7.6	95.7%
AOS_1c		57.56	91%	0.98704	1.512	93.034	-8.45	97.8%

Table (2): Prediction of Heme and Active Site Residues

	Pocket	Area Å²	Volume Å³	Pocket Residues	Mouth Openings	HEM-Binding Residues
AOS2b	Pocket 1 (green)	1523.9	1968.5	6 9 10 11 28 29 31 33 39 43 46 49 50 100 119 122 123 126 129 130 131 132 133 192 193 195 196 197 199 200 201 202 203 204 257 261 262 263 264 265 266 267 295 331 332 333 342 344 345 346 347 348 349 352 353 377 378 379 380	3	6K 10F 28C 29L 43K 46L 50L 100Y 196N 197S 200G 204L 262P 266Q 331W 333N 344N 345K 347C 348P 352F 353V
	Pocket 2 (purple)	804.8	1966.1	1 3 4 6 33 266 267 268 274 275 276 277 278 280 285 291 292 293 294 295 297 298 299 301 303 304 328 330 333 334 335 338 344 345 346	1	
	Pocket 3 (blue)	498.6	654.8	47 50 51 53 54 55 57 58 237 238 239 240 243 246 340 348 351 352 354 355 358 359 362	2	
AOS1c	Pocket 1 (brown)	3355.6	4086.9	56 57 58 62 63 67 83 84 89 115 118 119 120 123 124 125 126 129 135 136 137 139 140 141 143 145 147 150 153 154 156 157 160 188 190 196 203 207 222 225 226 229 230 231 232 233 234 235 236 237 238 239 240 241 242 243 247 248 251 252 255 256 257 259 297 300 301 302 303 304 305 306 307 308 309 310 311 312 313 314 366 369 370 371 372 373 374 375 376 401 403 404 405 439 440 441 448 450 452 453 454 455 456 457 458 459 460 461 464 482 483 484 485 486 487 488 489 490 491 493	10	115K 119F 136L 137S 146H 150K 153L 157L 305N 306S 309G 310M 313L 371P 375Q 439W 441N 452D 453K 454Q 455C 456A 457G 460F 461V

Table (3): Catalytic Residues Involved In Complex Formation

Substrate	Domain	Catalytic Residues
13(S)-HPODE	Reference Model	Phe 92, Leu 126, Leu 130, Tyr 180, Ala 272, Asn 276, Thr 277, Pro 343, Val 344, Trp 410, Asn 412, Cys 426, Ala 427, Gly 428, Phe 431, Val 432
	AOS2b	Leu 46, Leu 49, Leu 50, Tyr 100, Ala 192, Asn 196, Ser 197, Gly 200, Leu 201, Val 263, Trp 331, Ser 332, Asn 333, Cys 347, Gly 349, Phe 352, Val 353
	AOS1c	Leu 118, Phe 119, Phe 304, Asn 305, Gly 308, Gly 309, Pro 371, Val 372, Met 374, Gln 375, Tyr 376, Trp 439, Asn 441, Lys 453, Val 461
9(S)-HPODE	Reference Model	Phe 92, Tyr 180, Phe 275, Asn 276, Thr 277, Gly 280, Val 344, Pro 346, Trp 410, Cys 426, Gly 428, Val 432
	AOS2b	Lys 6, Phe 10, Thr 11, Leu 126, Leu 129, Phe 195, Asn 196, Gly 199, Gly 200, Val 203, Pro 262, Val 263, Phe 265, Trp 331, Asn 333
	AOS1c	Lys 115, Leu 118, Phe 119, Thr 120, Ser 137, Leu 233, Val 372, Met 374, Gln 375, Tyr 376, Asn 441, Lys 453, Gln 454, Cys 455
13(S)-HpOTrE	Reference Model	Phe 92, Leu 126, Tyr 180, Ala 272, Phe 275, Asn 276, Thr 277, Gly 280, Pro 343, Val 344, Gln 347, Trp 410, Ser 411, Asn 412, Cys 426, Gly 428, Val 432
	AOS2b	Phe 10, Leu 29, Phe 195, Asn 196, Gly 199, Gly 200, Val 203, Pro 262, Val 263, Lys 264, Gln 266, Trp 331, Asn 333, Lys 345, Cys 347, Leu 380, Gly 381
	AOS1c	Phe 119, Ser 137, Leu 153, Phe 300, Ala 301, Asn 305, Ser 306, Gly 309, Pro 371, Val 372, Trp 439, Asn 441, Cys 455, Ala 456, Val 461

Figure captions

- **Fig. (1):** Neighbor-joining phylogenetic tree of our AOS domains amino acid sequences relative to published sequences with highest degree of homology.
- **Fig. (2):** Multiple alignments of AOS2b and 1c protein sequences with top matching sequences of P450 superfamily showing the conservation of P450 domain (residues in red). The conserved domain in AOS2b lies between residues 217-352 **(A)** and in 1c between residues 331-477 **(B)**.
- **Fig. (3):** Superimposition of our AOS2b **(A)** and 1c **(B)** with crystal structure of *Arabidopsis thaliana* allene oxide synthase cytochrome P450, CYP74A complexed with 13(S)-HOT (PDB: 3dsi. Chain A). Our models are colored in red and the template model in blue.
- **Fig. (4):** Quality assessment and validation of our modeled AOS proteins. **(5.A, C)** show Z-score plot for AOS2b and AOS1c models respectively; **(5.B, D)** show Ramachandran plot of residues in the most favorable region and disallowed regions for AOS2b and AOS1c respectively.
- **Fig (5):** Ribbon diagram of the AOS2b **(A)** and AOS1c **(C)** structures showing the identification of P450 superfamily domains (pink) as viewed in POLYVIEW-3D. Heme- ligand is shown as gray spheres; hem-iron in green and the binding residues are colored in blue. Conserved residues are colored in red, and heme-binding loop (red) is indicated by black arrows, conserved Cys residues are shown in figures **(B, D).**
- **Fig. (6):** Predicted ligand binding sites (pockets) of our models colored according to secondary structure as viewed in Chimera viewer; helices in orange, strands in purple and loops in gray. The largest pockets in AOS2b **(A)** are colored in green and brown respectively, and in AOS1c **(B)** the major pocket is displayed in brown.
- **Fig. (7):** Binding poses of screened substrates. Protein models are colored according to secondary structure elements, where helices in orange, strands in purple and loops in gray, heme-cofactor is colored in green. The top panel shows the transposition of 13(S)-HPODE **(A),** 9(S)-HPODE **(B)** and 13(S)-HpOTrE **(C)** in reference (3dan) model., the middle panel shows the transposition of the same substrates respectively in modeled AOS2b **(D, E and E)**, and the lower panel show their transposition in modeled AOS1c **(G, H and I)**. Distance between 9/13C-Oxygen and heme-iron is demonstrated.
- **Fig. (8):** Full fitness scores **(A)** and relative binding energies **(B)** of 13(S)-HPODE, 9(S)-HPODE and 13(S)-HpOTrE docked in modeled AOSs comparing to reference structure (PDB:3dan).
- **Fig. (9):** Binding residues interactions with screened substrates in modeled AOSs comparing to reference model 3dan.

Figure 1

(A)

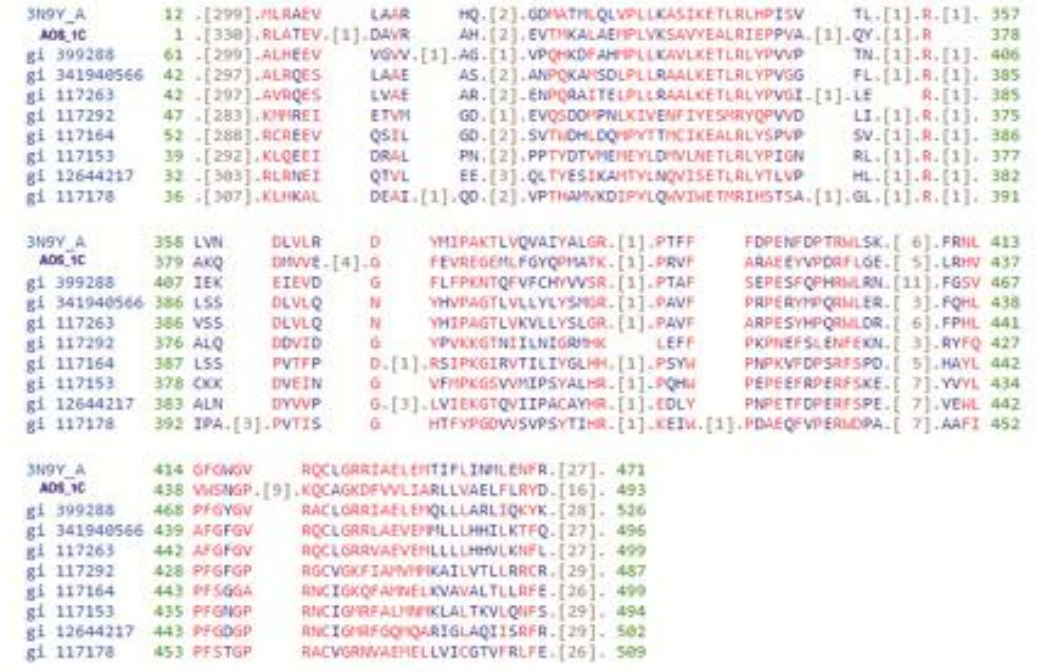

(B)

Figure 2

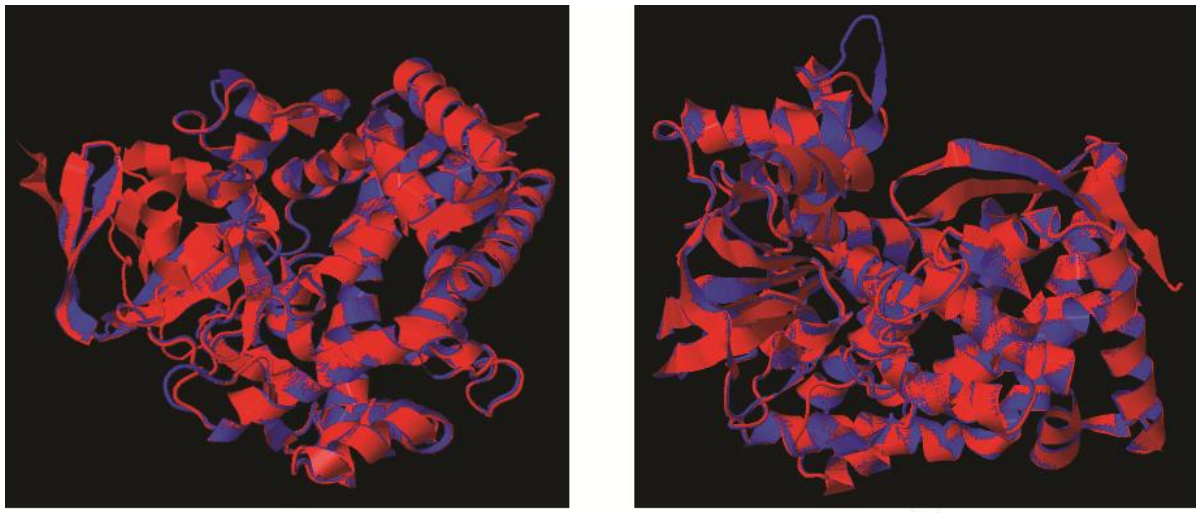

(A) (B)

Figure 3

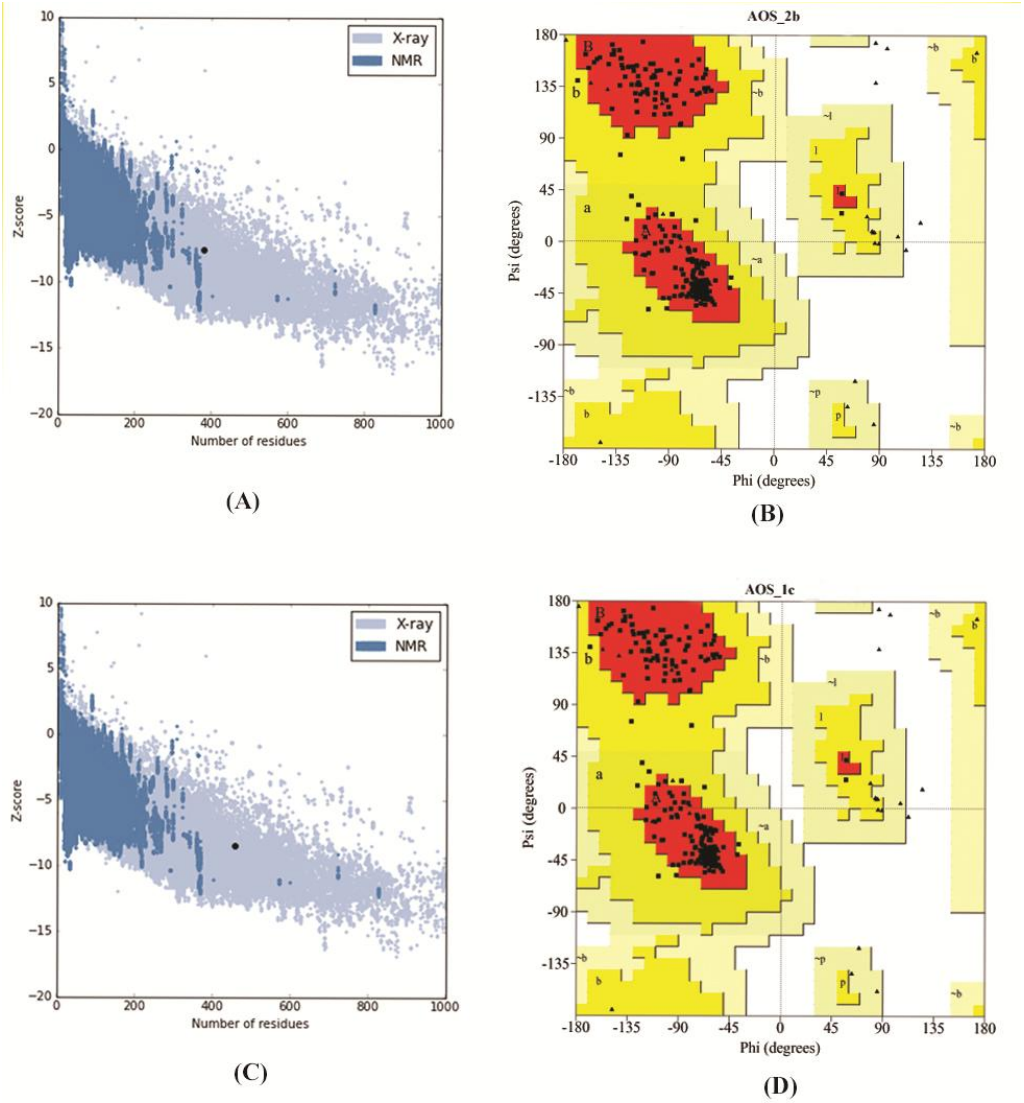

Figure 4

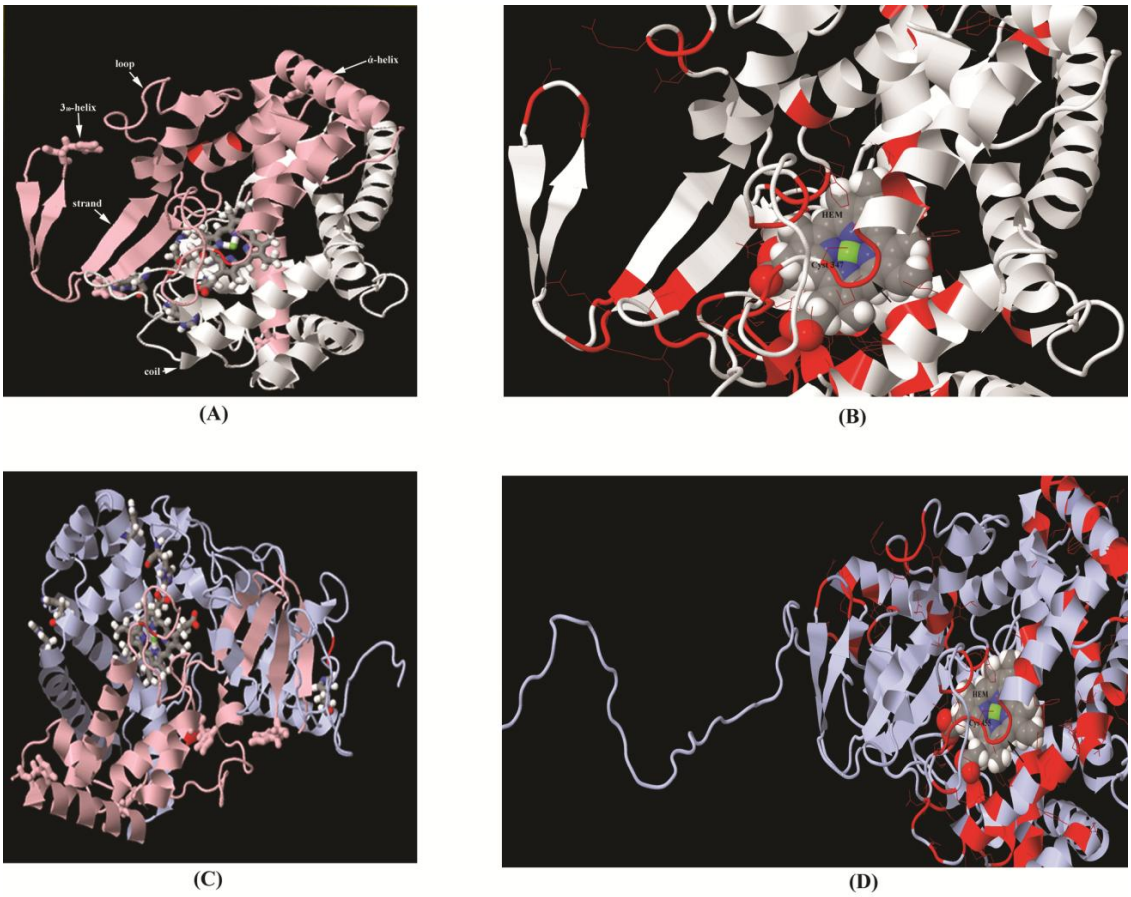

Figure 5

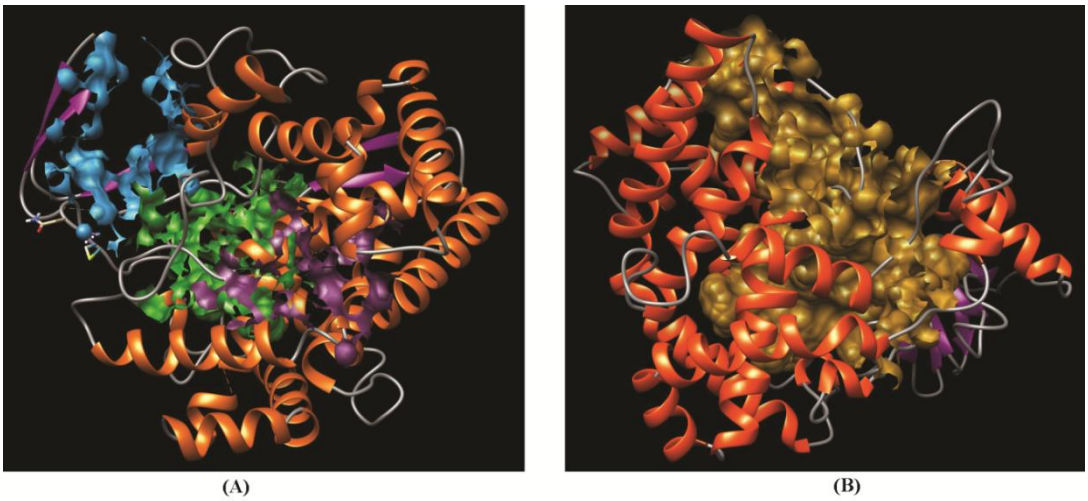

Figure 6

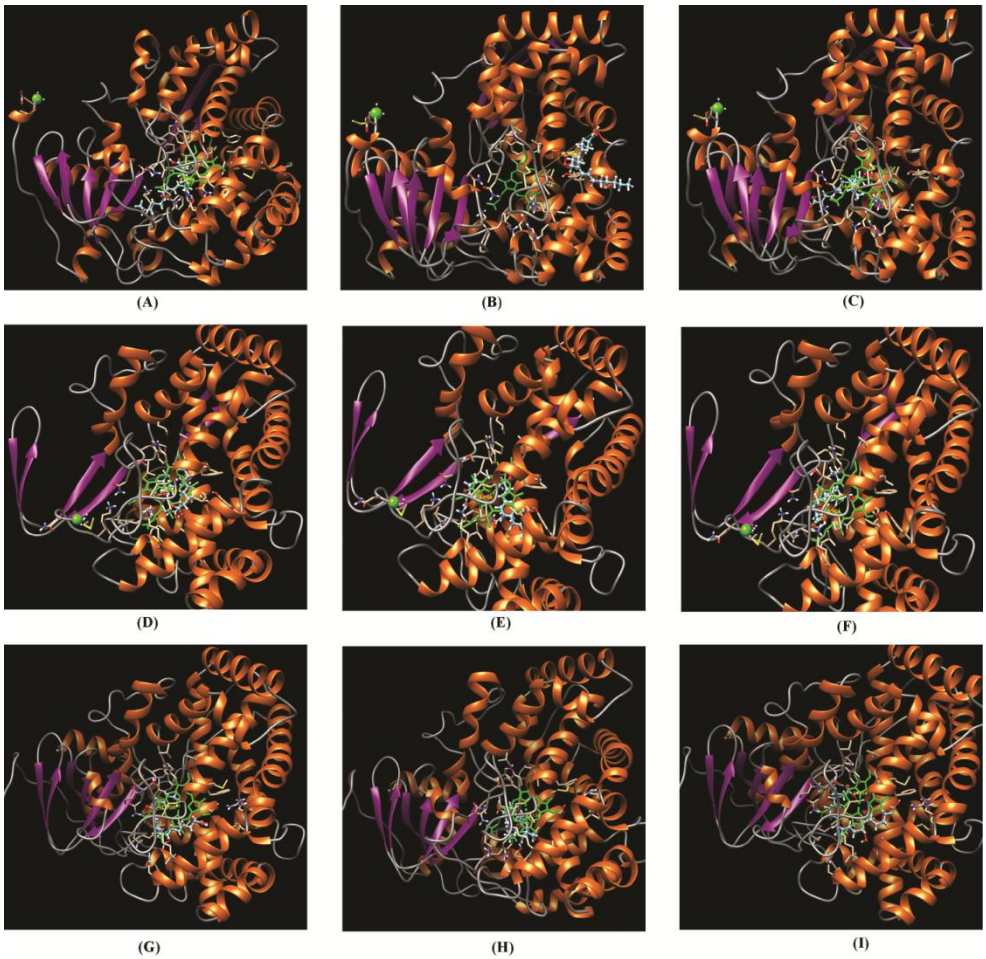

Figure 7

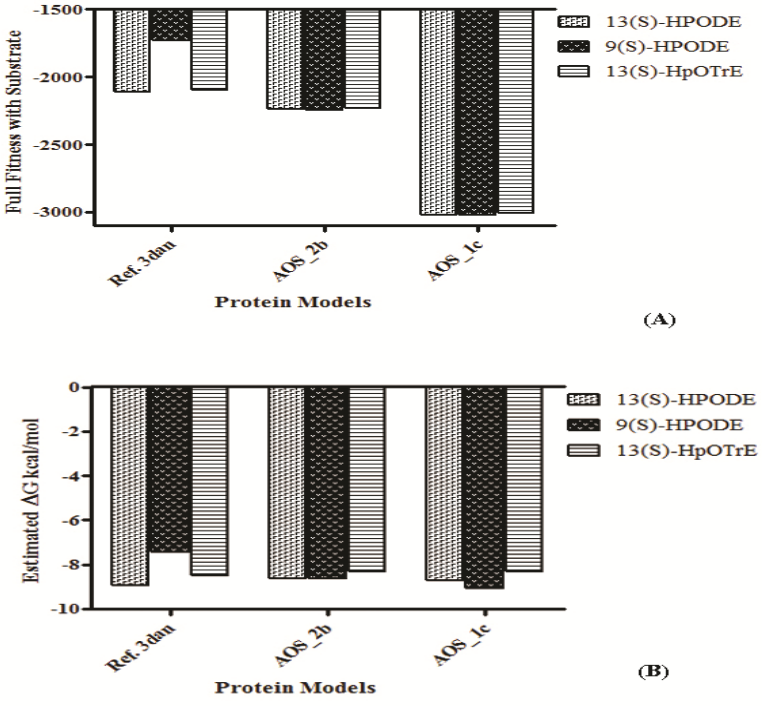

Figure 8

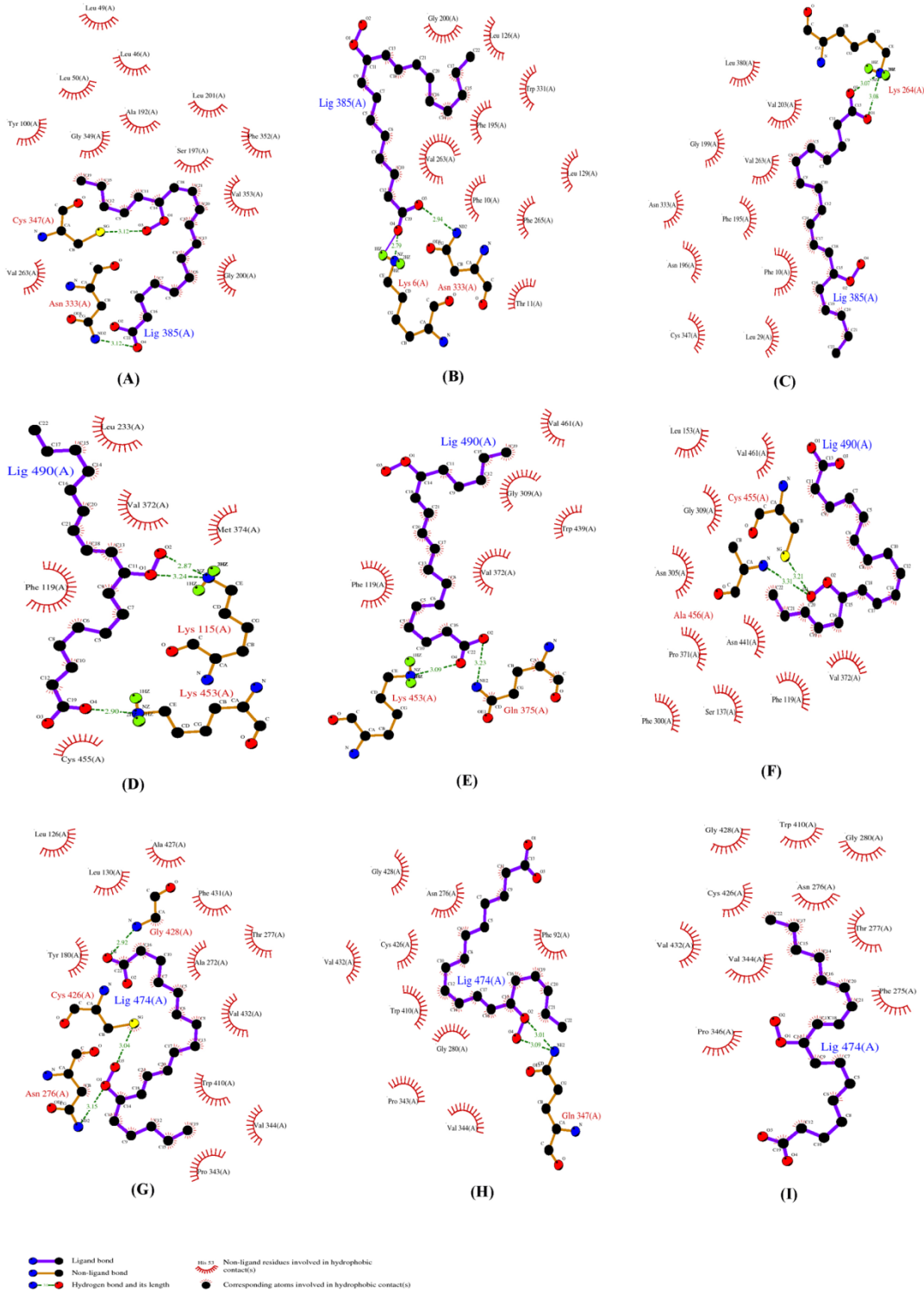

Figure 8

Eman Wahba Elgammal " In-Silico Analysis, Catalytic Site and Substrate Specificity Prediction of Two Phylogenetically Distinct Zea mays Allene Oxide Synthases" IOSR Journal of Pharmacy and Biological Sciences (IOSR-JPBS) 14.1 (2019): 08-20.